Comparison of Penetratin and Other Homeodomain-Derived Cell-Penetrating Peptides: Interaction in a Membrane-Mimicking Environment and Cellular Uptake Efficiency†

Stéphane Balayssac,‡ Fabienne Burlina,* Odile Convert, Gérard Bolbach, Gérard Chassaing, and Olivier Lequin*

Synthèse, Structure et Fonction de Molécules Bioactives, UMR 7613 CNRS, Université Pierre et Marie Curie, boîte 45, 4 place Jussieu, 75252 Paris Cedex 05, France

Received September 10, 2005; Revised Manuscript Received December 1, 2005

ABSTRACT: Antennapedia and other homeoproteins have the unique ability to efficiently translocate across biological membranes, a property that is mediated by the third helix of the homeodomain. To analyze the effects of sequence divergence in the homeodomain, we have compared the cellular uptake efficiencies and interaction properties in a membrane-mimicking environment of four peptides corresponding to the third helix sequence of Antennapedia, Engrailed-2, HoxA-13, and Knotted-1. NMR studies revealed that these peptides adopt helical conformations in SDS micelles. Their localization with respect to the micelle was investigated using Mn^{2+} as a paramagnetic probe. Peptides are positioned parallel to the micelle surface, but subtle differences in the depth of immersion were observed. Using a recently developed method for quantification of CPP cellular uptake based on MALDI−TOF mass spectrometry, all of these peptides were found to translocate into cells but with large differences in their uptake efficiencies. The peptide with the highest uptake efficiency was found to be the least deeply inserted within the micelle, indicating that electrostatic surface interactions may be a major determinant for membrane translocation. A new cell-penetrating peptide derived from Knotted-1 homeodomain with improved uptake properties compared to penetratin is introduced here.

Homeoproteins form a large family of transcription factors characterized by a conserved DNA-binding motif called homeodomain (*1*). They are involved in the development program of organisms by modulating expression patterns of target genes in a tissue-specific, spatio-temporal manner. The conserved homeodomain adopts a three-helical fold, with a characteristic helix−turn−helix topology. The third helix constitutes the main DNA recognition site and binds to the major groove of DNA. Despite a strong genetic conservation of the homeodomain, homeoproteins have diverged to acquire different DNA-binding specificities and different regulation properties mediated by specific protein−protein interactions.

Another striking property of several homeodomains is the ability to translocate efficiently through biological membranes with a low lytic activity, by a yet nonfully elucidated mechanism. The *Drosophila* Antennapedia homeodomain was the first translocating homeodomain to be discovered (*2*), and the same property was also reported for Engrailed (*3*), HoxA-5 (*4*), HoxB-4 and HoxC-8 (*5*), and PDX-1 (*6*). The third helix of the homeodomain has been shown to be responsible for cellular internalization. The peptide corresponding to the third helix of *Drosophila* Antennapedia homeodomain (residues 43−58), also known as penetratin, was the first cell-penetrating peptide (CPP)[1] to be discovered (*7*) and has been extensively used to deliver biologically active cargoes into cells (*8*). The use of penetratin variants has shown that the translocation process does not imply chiral recognition by a receptor and that the helical secondary structure induced in membrane-mimicking environments is not required either (*9*, *10*). Thus, these low structural requirements together with the high sequence conservation of the homeodomain suggest that internalization properties should be shared among the whole homeoprotein family. The positive charge of the third helix plays an important role because the removal of a single positive charge by Ala scanning in penetratin sequence decreases the membrane-binding affinity and the cellular uptake of penetratin variants (*11*, *12*). The C-terminal segment of the peptide which is rich in basic residues is crucial for internalization. The truncation of the four C-terminal residues inhibits uptake, whereas the peptide corresponding to residues 52−58 retains

† This study was supported in part by grants from FNS and CNRS (ACI "Dynamique et Réactivité des Assemblages Biologiques" 04/030) and from INTAS (international association for the promotion of cooperation with scientists from the new independent states of the former Soviet Union).

* To whom correspondence should be addressed. E-mail: burlina@ccr.jussieu.fr (F.B.); lequin@ccr.jussieu.fr (O.L.). Telephone: 33 1 44 27 31 15. Fax: 33 1 44 27 38 43.

‡ Present address: Magnetic Resonance Center (CERM) and Department of Chemistry, University of Florence, Via Luigi Sacconi 6, 50019 Sesto Fiorentino (FI), Italy.

[1] Abbreviations: Antp, Antennapedia homeodomain third helix (penetratin); Boc, *tertio*butyloxycarbonyl; CPP, cell-penetrating peptide; CSD, chemical-shift deviation; DQF-COSY, double-quantum-filtered correlation spectroscopy; Eng, Engrailed-2 homeodomain third helix; Hox, HoxA-13 homeodomain third helix; Kno, Knotted-1 homeodomain third helix; NMR, nuclear magnetic resonance; NOE, nuclear Overhauser effect; NOESY, NOE spectroscopy; SEM, standard error of the mean; SDS, sodium dodecyl sulfate; TOCSY, total correlation spectroscopy.

10.1021/bi0518390 CCC: $33.50
Published on Web 01/10/2006

Table 1: Peptide Sequences Corresponding to the Third Helix of Selected Homeodomains[a]

Peptide	Sequence[b]	Origin[c]
Antp	R **Q** I K I **W** **F** Q **N** R **R** M K W K **K**-NH_2	Drosophila Antennapedia
Eng	S **Q** I K I **W** **F** Q **N** K **R** A K I K **K**-NH_2	Human Engrailed 2
Hox	R **Q** V T I **W** **F** Q **N** R **R** V K E K **K**-NH_2	Human HoxA13
Kno	K **Q** I N N **W** **F** I **N** Q **R** K R H W **K**-NH_2	Maize Knotted 1

[a] Peptides used in the cell internalization assays possess a biotin-$(Gly)_4$ N-terminal extension. Hox and Kno peptides used in NMR studies were acetylated at their N terminus. [b] Conserved residues in the four sequences are shown in bold. [c] Antp, Eng, and Hox peptides correspond to residues 43−58 of the homeodomain (residue numbering in Swissprot entries: ANTP_DROME, 339−354; HME2_HUMAN, 286−301; HXA13_HUMAN, 364−379). Kno corresponds to residues 46−61 of the homeodomain (KN1_MAIZE, 309−324) because of a three amino acid insertion; for the sake of clarity, the same 43−58 numbering was used.

60% of the full-length penetratin uptake efficiency (*7*, *11*). Hydrophobic residues are also critical because deletion of Trp48 and Phe49 in Antennapedia homeodomain abolishes its internalization (*13*). Moreover, the substitution of Trp48 by Phe in penetratin strongly impairs its cellular uptake. The role of Trp56 is more controversial (*7*, *11*, *12*). All of these data suggest that a subtle balance between hydrophobic and positively charged residues may affect the interaction with membranes and the translocation process.

The aim of this study was to analyze to what extent sequence divergence of the third helix might modulate the properties of these CPPs. Beside Antennapedia, the third helices of Islet-1 (*14*) and PDX-1 (*15*) have also been found to translocate efficiently across the cell membrane. The alignment of the third helix sequences of several homeodomains led us to select four peptides, on the basis of charged and hydrophobic residue distributions (Table 1). We chose the third helix of Engrailed-2 (Eng), which is very close to penetratin, regarding the distribution of hydrophilic and hydrophobic residues, but contains one basic residue less at the N terminus and has an Ile residue instead of a Trp in position 56. The third helix of HoxA-13 (Hox) was selected to study the impact of a negative charge in the C-terminal segment of the third helix. No data on the internalization of this homeoprotein have been reported thus far. Finally, we also examined the third helix of Knotted-1 (Kno), a maize homeoprotein, which possesses the most divergent sequence compared to the other third helices. The Knotted-1 homeodomain was found to efficiently transfer between animal cells (*16*).

We have compared the cellular uptake efficiencies and interaction properties in a membrane-mimicking environment of these four homeodomain-derived peptides to identify the critical molecular features for membrane translocation. The conformation of the four peptides was first analyzed by nuclear magnetic resonance (NMR) spectroscopy using sodium dodecyl sulfate (SDS) micelles as a model of the water/membrane interface. Their localization with respect to the micelle was investigated using a hydrosoluble paramagnetic probe and revealed subtle differences in positioning. Using a matrix-assisted laser desorption ionization−time-of-flight mass spectrometry (MALDI−TOF MS) assay recently developed in our group (*17*) that enables an accurate measurement of the internalized amounts, we found that all of these peptides translocate into cells but with large differences in their uptake efficiencies.

EXPERIMENTAL PROCEDURES

Peptide Synthesis. Standard *tertio*butyloxycarbonyl (Boc) amino acids, *p*-methylbenzhydrylamine-polystyrene resin (0.9 mmol NH_2/g), and *O*-(benzotriazol-1-yl)-1,1,3,3-tetramethyluronium hexafluorophophate (HBTU) were purchased from Senn Chemicals (Dielsdorf, Switzerland). [2,2-D_2, 98%]-*N*-Boc-Glycine was obtained from Euriso-top (Saint-Aubin, France). Solvents (peptide synthesis grade) and other reagents were obtained from Applied Biosystems. Peptides were assembled by stepwise solid-phase synthesis on a ABI Model 433A peptide synthesizer (Applied Biosystems) using a standard Boc strategy (amino acid activation with dicyclohexylcarbodiimide/1-hydroxybenzotriazole or HBTU), on a 0.1 mmol scale. After synthesis of the CPP domain, the peptidyl resin was separated into three batches; two batches were further elongated by either four nondeuterated or four deuterated glycine residues followed by a biotin to give the H-CPPs and D-CPPs, respectively. Peptides were cleaved from the resin by treatment with anhydrous HF (1 h, 0 °C) in the presence of anisole (1.5 mL/g peptidyl resin) and dimethyl sulfide (0.25 mL/g peptidyl resin). They were purified by preparative reverse-phase HPLC on a C8 column, using a linear acetonitrile gradient in an aqueous solution of 0.1% (v/v) trifluoroacetic acid. Peptides were obtained with a purity >95%, as assessed by analytical HPLC. The peptide identity was checked by MALDI−TOF mass spectrometry (Voyager Elite, PerSeptive Biosystems) using α-cyano-4-hydroxycinnamic acid matrix.

NMR Spectroscopy. NMR samples were prepared by dissolving lyophilized peptides to a 2 mM concentration in 550 μL of 90:10 H_2O/D_2O in the presence of 120 mM SDS-d_{25} (purchased from Euriso-top). The pH was adjusted to 4.6 using microliter amounts of HCl (0.25 or 0.5 M). Sodium 3-(trimethylsilyl)-propionate-2,2,3,3-d_4 was used as an internal reference for ^{1}H chemical-shift calibration. NMR experiments were recorded at 45 °C on Bruker Avance spectrometers operating at a ^{1}H frequency of 500 MHz and were processed with Bruker XWIN-NMR software running on a SGI O2 workstation. Spectra were analyzed with the aid of XEASY (*18*). Proton assignments were obtained from the analysis of 2D total correlation spectroscopy (TOCSY) (clean MLEV-17 isotropic mixing scheme of 18−80 ms duration) (*19*, *20*) and 2D waterflipback NOE spectroscopy (NOESY) (200−250 ms mixing time) experiments (*21*, *22*). Solvent suppression was achieved with a WATERGATE sequence (*23*). The assignment of side-chain protons was also based on the analysis of either 2D double-quantum-filtered correlation spectroscopy (DQF-COSY) (*24*) or 2D TOCSY recorded with short mixing times (∼20 ms). Two-dimensional experiments were typically collected as 512 (t_1) × 2048 (t_2) time-domain matrices over a spectral width of 12 ppm, with 64 scans per t_1 increment. The time-domain data were multiplied by 60°-shifted square sinebell window functions and zero-filled prior to Fourier transformation. Baseline distortions were corrected with a fifth-order polynomial function. $^3J_{H^N-H^\alpha}$ coupling constants were extracted using INFIT (*25*) from 2D NOESY spectra recorded with a

long acquisition time in the t_2 dimension (340 ms). The kinetics of amide proton exchange was followed by recording 1D spectra at 30 °C over the time course of a few hours after solubilization of lyophilized peptide/SDS samples in D_2O. The chemical-shift deviation (CSD) of H^α protons was calculated using the set of random-coil values reported in water (*26*).

Titration Experiments with $MnCl_2$. Titration experiments were carried out by stepwise additions of $MnCl_2$ from 1, 10, and 100 mM stock solutions in water. The relaxation enhancements were monitored by recording 1D spectra after each addition of the paramagnetic cation (Mn^{2+} concentrations of 0.2, 0.5, 1, 1.5, 2, and 4 mM). Two-dimensional TOCSY experiments were also collected as 360 (t_1) × 2048 (t_2) time-domain matrices over a spectral width of 6000 Hz, with 64 scans per t_1 increment and an isotropic mixing time of 62 ms.

Structure Calculations. Interproton distance upper limits were constrained to 2.8, 3.0, 3.5, 4.0, 4.5, 5.0, and 5.5 Å, depending upon NOESY cross-peak intensities. The lower bounds were set to the sum of the van der Waals radii of two protons (1.8 Å). Pseudoatoms were introduced for distances involving equivalent protons, and upper limits were corrected appropriately (*27*). The ϕ torsion angle was restrained to [−80°, −30°] for ${}^3J_{H^N-H^\alpha} \leq 5.5$ Hz and to [−180°, −30°] for $5.5 < {}^3J_{H^N-H^\alpha} \leq 6.5$ Hz [positive ϕ values were discarded in the absence of very strong intraresidual $d_{\alpha N}$ nuclear Overhauser effect (NOE) (*28*)]. Structures were calculated using DYANA (*29*) and XPLOR-NIH (*30*) programs running on SGI O2 R10000 workstations. A set of 100 structures was generated by torsion-angle dynamics in DYANA using a standard simulated annealing protocol (*29*). The best 20 structures were then subjected to conjugate-gradient minimization within XPLOR-NIH using CHARMM22 force field. The nonbonded interactions were calculated with a 12 Å cutoff, using a Lennard−Jones potential for the van der Waals term and a distance-dependent dielectric function ($\epsilon = \epsilon_0\epsilon_r$ with a relative permittivity of $\epsilon_r = 4r$) for the electrostatic energy. Structures were visualized using InsightII version 98 program (Accelrys, Inc., San Diego, CA). The structure quality was assessed with PROCHECK-NMR (*31*).

Measurement of the Amount of Internalized CPP by MALDI−TOF MS. The internalization experiments were performed using 12-well plates. In each well, 10^6 adherent CHO K1 cells were incubated for 75 min at 37 °C with a 1 mL culture medium (Dulbecco's modified eagle medium) containing the biotinylated nondeuterated CPP (H-CPP) (7.5 μM). The cells were then washed 3 times with a 2 mL culture medium, treated for 3 min at 37 °C with 500 μL of a solution containing 0.05% trypsin and 0.02% EDTA, and transferred at 4 °C. Soybean trypsin inhibitor (100 μL, 5 mg/mL) and bovine serumalbumin (BSA) (100 μL, 1 mg/mL) were added. The cell suspension was transferred in a 1.5 mL conic tube, and the well was washed with 500 μL of 50 mM Tris-HCl buffer (pH 7.4). Both suspensions were pooled and centrifuged for 2 min at 3000 rpm. The pellet containing the intact cells was washed with 1 mL of 50 mM Tris-HCl buffer (pH 7.4) and 0.1% BSA (buffer A) and centrifuged again. The pellet was mixed with a known amount of the adequate biotinylated deuterated CPP (D-CPP) and 150 μL of a solution containing 0.3% Triton X100 and 1 M NaCl. The mixture was heated for 15 min at 100 °C. The cell lysate was then centrifuged for 5 min at 10 000 rpm at 4 °C. The supernatant was mixed with 850 μL of buffer A. The mixture was incubated for 2 h at 4 °C with 100 μg of streptavidin-coated magnetic beads (Dynabeads M-280, Dynal, France) to capture the biotinylated peptides. After bead immobilization with the Dynal magnetic particule concentrator, the supernatant was removed. Beads were washed twice with buffer A (200 μL), twice with buffer A containing 0.1% sodium dodecyl sulfate (200 μL), twice with buffer A containing 1 M NaCl (200 μL) and finally with water (2 × 200, 2 × 100, 3 × 50, and 3 × 10 μL). Beads were mixed with 3 μL of a saturated solution of α-cyano-4-hydroxycinnamic acid (HCCA) in acetonitrile/water−0.1% trifluoroacetic acid (4:1), and 1 μL of the mixture was deposited on the MALDI−TOF sample holder. The samples were analyzed by MALDI−TOF MS (ion positive reflector mode) on a Voyager Elite PerSeptive Biosystems mass spectrometer or a 4700 Applied Biosystems MALDI−TOF−TOF mass spectrometer. The laser fluence used was near the threshold of peptide ion production for the considered deposits (bead-associated peptide covered with HCCA matrix). Spectra were averaged from several hundred laser shots recorded on different spots of the deposit to get reliable statistics on the peak area (*17*). The area of the $[M + H]^+$ signals including all of the isotopes of the H-CPP and D-CPP species were measured. In the first experiment, the amount of internalized peptide was evaluated for each CPP by adding various and known amounts of the adequate D-CPP to samples containing the internalized peptide. The amount of D-CPP added in the subsequent experiments was chosen to get a peptide ratio close to 1:1 to allow a precise quantification. The internalization experiments were performed in duplicates and repeated at least 4 times independently.

RESULTS

NMR Spectroscopy of Homeodomain-Derived Peptides in Micellar SDS. The NMR spectra of the four homeodomain-derived peptides Antp, Eng, Hox, and Kno were recorded in the presence of SDS micelles using the same concentrations of peptide (2 mM) and SDS (120 mM). Assuming that the SDS micelles comprise about 60 molecules (*32*), these experimental conditions correspond to a peptide/SDS micelle ratio of 1:1. A high temperature of 45 °C was chosen in these studies to limit the broadening of proton line widths caused by SDS and record good-quality 2D NMR spectra. The proton chemical shifts of the four homeodomain-derived peptides were assigned using a conventional strategy based on homonuclear 2D experiments (*33*) and are listed in Tables S1−S4 as Supporting Information. Antp peptide has been the subject of several NMR studies in different solvents [water/alcohol mixtures (*10*, *34*), SDS micelles (*10*, *35*, *36*), small nonaligned isotropically tumbling phospholipid bicelles (*36*−*38*)]. The ^1H chemical shifts of Antp are very close to those previously reported in SDS micelles using slightly different pH values and concentrations, with most of them falling within 0.04 ppm of the reported values (*35*).

Information on the secondary structure of the peptides can be inferred from the CSDs of H^α protons, calculated as the differences between experimentally observed chemical shifts and corresponding random-coil values determined in water (Figure 1). Negative values of H^α CSDs, corresponding to

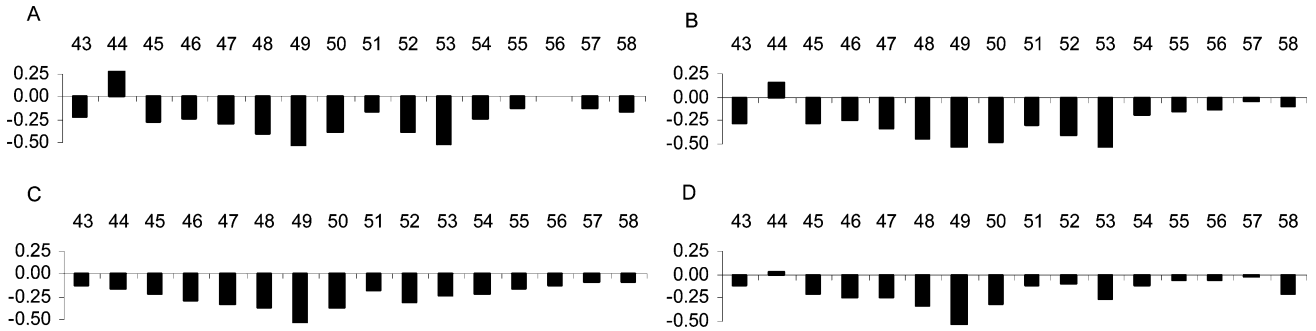

FIGURE 1: H^{α} CSDs for Antp (A), Eng (B), Hox (C), and Kno (D) peptides in the presence of SDS micelles. The CSDs were calculated as the differences between observed chemical shifts and corresponding random-coil values in water (*26*).

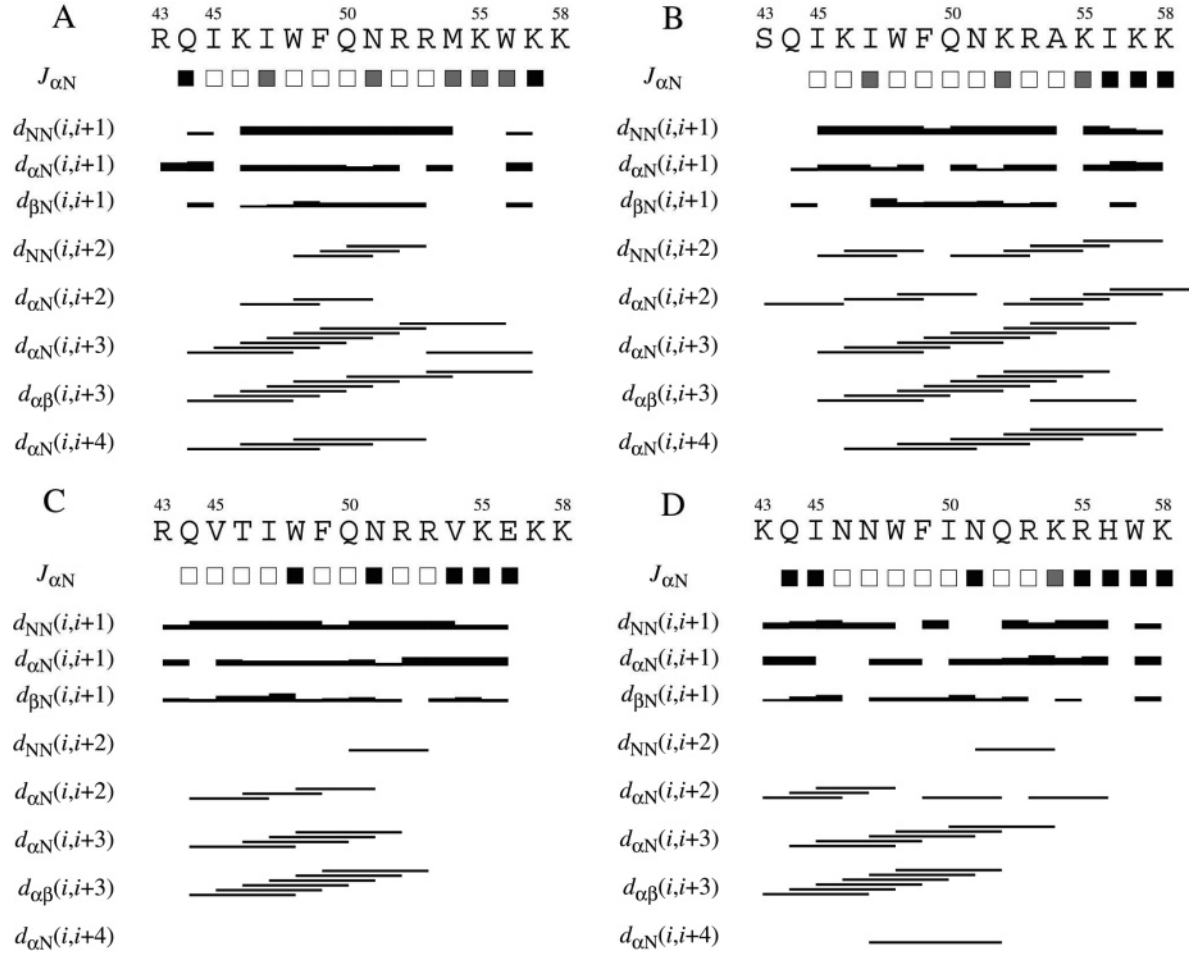

FIGURE 2: Summary of sequential (i, $i+1$) and medium-range (from i, $i+2$ to i, $i+4$) NOEs and $^3J_{H^N-H^{\alpha}}$ coupling constants observed for Antp (A), Eng (B), Hox (C), and Kno (D) peptides in the presence of SDS micelles. $^3J_{H^N-H^{\alpha}}$ coupling constants are represented by squares: open square, $3.5 \leq J \leq 5.5$ Hz; gray square, $5.5 < J \leq 6.5$ Hz; filled square, $6.5 < J \leq 7.5$ Hz. The relative intensity of NOE connectivities is indicated by horizontal bars of varying thickness.

upfield shifts of H^{α} protons, are observed throughout the sequences of the four peptides. This indicates that these homeodomain-derived peptides tend to adopt helical conformations in this micellar environment. On the basis of the average H^{α} CSD calculated for residues 45−58, the helical propensity decreases in the order Eng > Antp > Hox > Kno (CSDs of −0.32, −0.29, −0.26, and −0.21, respectively). The positive CSD value observed in position 44 for Antp, Eng, and Kno enables us to delineate the beginning of the helical segment at position 45 in the N terminus. For each peptide, the most negative CSD values are observed around positions 48−50, encompassing the two conserved Trp and Phe residues (Table 1). Gradually weaker negative values are observed toward the C terminus of each peptide, indicating a lower helical propensity.

The magnitude and pattern of sequential and medium-range NOEs together with $^3J_{H^N-H^{\alpha}}$ coupling constants also yield information on the secondary structure of the peptides. NOE correlations characteristic of the α-helical conformation are observed, including strong dNN(i, $i+1$) and medium dαN(i, $i+1$) sequential NOEs, together with numerous dαN(i, $i+3$), dαβ(i, $i+3$), and dαN(i, $i+4$) medium-range connectivities (Figure 2). Furthermore, many residues exhibit $^3J_{H^N-H^{\alpha}}$ coupling constants lower than 6 Hz (Figure 2), consistent with a preferential localization in the α_R region of the Ramachandran diagram.

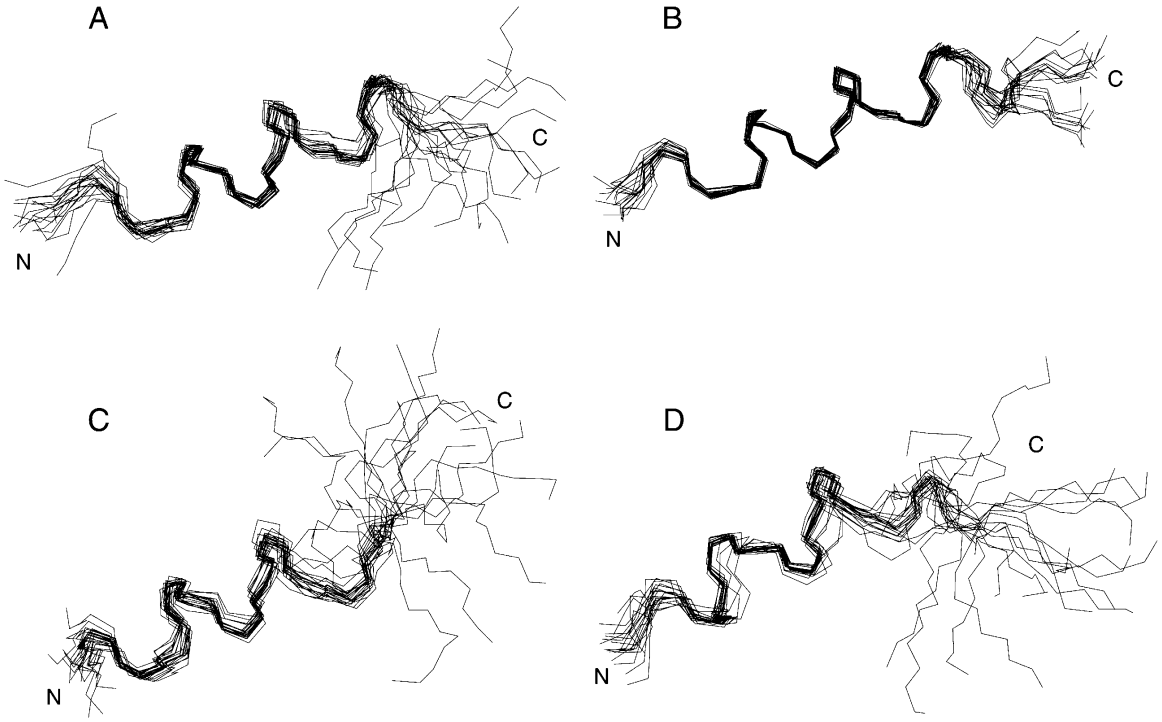

FIGURE 3: Three-dimensional solution structures of Antp (A), Eng (B), Hox (C), and Kno (D) peptides. Structures were superimposed by fitting the backbone atoms N, C^{α}, and C′ from residues 45 to 55.

Three-Dimensional Structures. The structures of the four homeodomain-derived peptides were calculated by simulated annealing using distance and ϕ dihedral angle constraints inferred from NOEs and $^3J_{H^N-H^{\alpha}}$ coupling constants, respectively. Structural statistics are provided in Table S5, available in the Supporting Information, and the structures represented by an ensemble of 20 models for each peptide are shown in Figure 3. The NMR structure families exhibit low energies and few residual violations, indicating a good agreement with experimental data. The quality and the definition of the NMR structures are correlated to the number of constraints used in the calculation. In particular, the Eng peptide, which exhibits the highest number of NOEs, adopts a well-defined helical structure around residues 45−55 (Figure 3), as shown by the low backbone root-mean-square deviation (rmsd) (0.36 Å). The conformations of N- and C-terminal residues are more disordered. Similarly, the Antp peptide forms a regular helix from residue 45 to 54, with residues 44 and 55−58 being more disordered. In the Hox peptide, the helical region spans residues 44−53, with the C-terminal segment being ill-defined. The helical domain is the shortest in the Kno peptide and encompasses residues 45−52 only.

Conformational Flexibility. Because the structure calculations are mainly based on the semiquantitative analysis of NOEs, the selected structures that represent the NMR ensemble may tend to give an overestimated view of the actual proportion of folded conformers. On the other hand, the H^{α} CSDs and $^3J_{H^N-H^{\alpha}}$ coupling constants are valuable parameters to detect conformational averaging. The definition of the secondary-structure elements observed in the calculated NMR structures is generally in good agreement with the H^{α} CSDs and $^3J_{H^N-H^{\alpha}}$ coupling constants. Residues 45−49 form the core of the helical structure, as confirmed by the large upfield shifts of H^{α} protons and numerous medium-range NOEs. Furthermore, the amide protons of residues Trp48 and Phe49 exhibit the slowest exchange kinetics in D_2O ($k_{ex} < 5 \times 10^{-3}$ min^{-1} at 30 °C). Therefore, these two protons are likely to be involved in stable hydrogen bonds. After this core helical structure, segment 50−52 in Antp and Hox peptides seems to exhibit more flexibility and/or conformational heterogeneity, as inferred from the increase of H^{α} CSD and the $^3J_{H^N-H^{\alpha}}$ coupling constant in position 51 and the lack of dαN(i, i + 3) and d$\alpha\beta$(i, i + 3) NOEs. The C-terminal portion of the four peptides is characterized by a greater conformational flexibility, as indicated by H^{α} CSDs closer to 0, $^3J_{H^N-H^{\alpha}}$ coupling constants around 6.5 Hz, and fewer medium-range NOEs. A few residual NOE violations are observed in the C-terminal segment of some structures (involving positions 56−57 in Eng and positions 52−53 in Hox), indicating that these NOEs cannot be simultaneously satisfied in a single conformer and that the C-terminal region displays conformational averaging. However, for Eng and Antp peptides, the C-terminal half remains largely helical.

Side-Chain Interactions. The conformation of the Trp48 side chain is well-defined, as evidenced by numerous NOEs involving aromatic side-chain protons. Residues Trp48 and Arg52 in Antp form π-stacking interactions, as shown by upfield shifts of Arg52 H^{δ} protons and NOEs with Trp48 aromatic protons. No NOEs were observed between Arg52 and Trp56, indicating that Arg52 preferentially interacts with Trp48. A π-stacking interaction was also observed between Phe49 and Arg53. In the other three peptides, similar i/i + 4 NOEs were observed, demonstrating side-chain interactions between Trp48, Phe49, and residues in position 52 and 53.

Location of Peptides in SDS Micelles. The position of the four homeodomain-derived peptides in the SDS micelles was examined using Mn^{2+} as a paramagnetic probe. The Mn^{2+} ion is located in the aqueous phase in the vicinity of anionic headgroups of SDS. The addition of this paramagnetic ion is known to cause selective broadening of resonances for residues exposed to the solvent or close to the water−micelle interface (*32*). The paramagnetic enhancements induced by

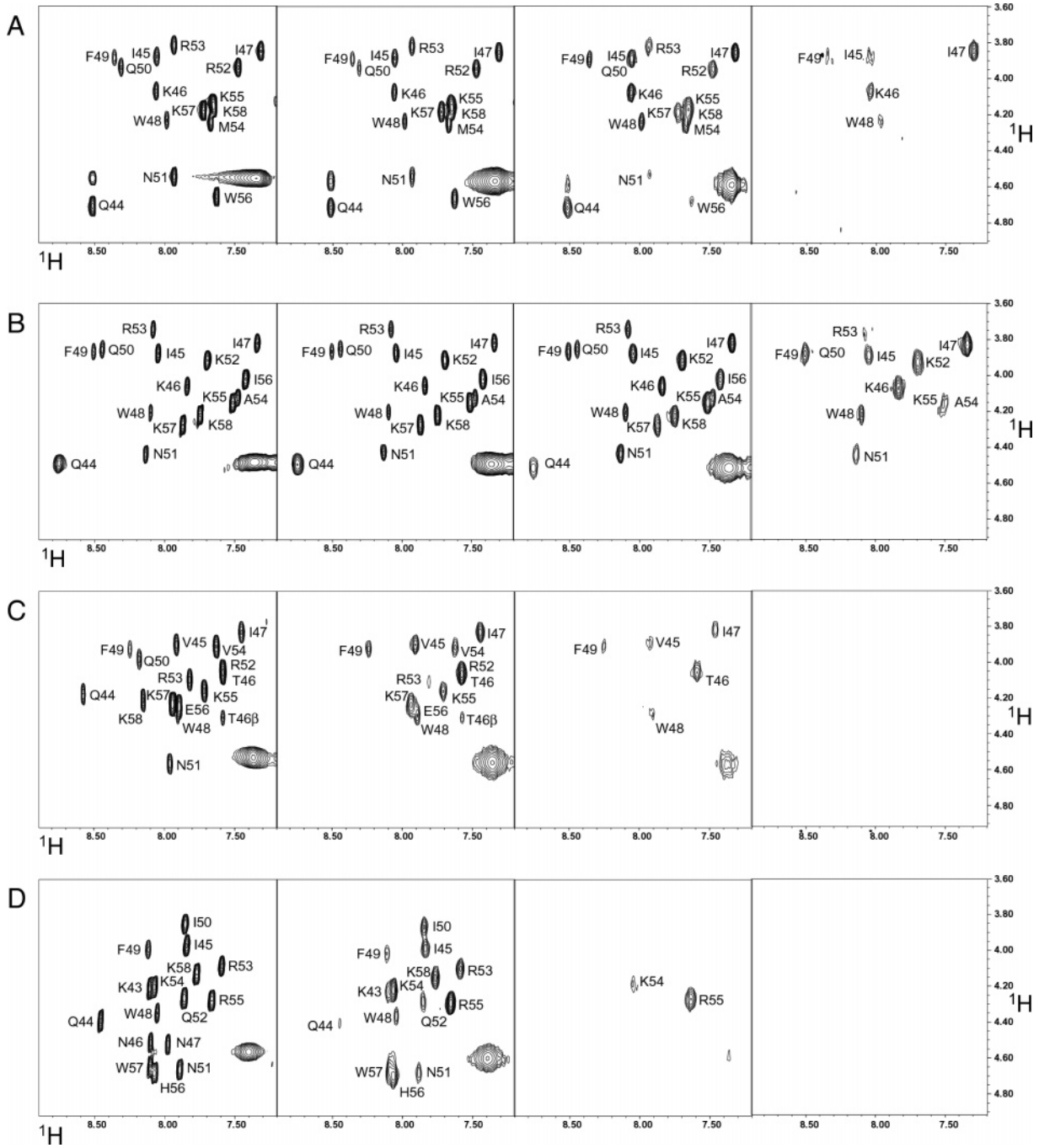

FIGURE 4: H^N-H^α region of 2D TOCSY spectra recorded in the presence of increasing concentrations of $MnCl_2$ for Antp (A), Eng (B), Hox (C), and Kno (D) peptides. The Mn^{2+} concentrations are from left to right: 0, 0.5, 1.5, and 4 mM. Correlations that are not annotated correspond to exchange peaks with the water resonance (4.60 ppm in the F1 dimension). The H^N-H^α correlation for the N-terminal residue in Antp and Eng peptides is not observed, owing to fast exchange of the amine group with the solvent.

stepwise additions of $MnCl_2$ up to 4 mM were monitored by measuring the residual amplitude of $HN-H^\alpha$ cross-peaks in 2D TOCSY spectra (Figure 4). The four homeodomain-derived peptides are differently affected by the paramagnetic Mn^{2+} probe. Indeed, many $HN-H^\alpha$ cross-peaks are still observed in the TOCSY spectrum of the Eng peptide upon the addition of 4 mM Mn^{2+}, whereas all $HN-H^\alpha$ correlations have disappeared for Hox and Kno peptides (Figure 4). These different sensitivities to the paramagnetic probe reflect variations in accessibility and consequently different burials within the SDS micelle. From the relaxation effects of the Mn^{2+} probe, it can be inferred that the depth of immersion within the SDS micelle increases in the order Eng > Antp > Hox > Kno. A comparison of the decay of $HN-H^\alpha$ cross-peaks of individual residues also yields information on the peptide orientation with respect to the SDS micelle. For each peptide, the $HN-H^\alpha$ correlations for the N- and C-terminal residues are not observed at a Mn^{2+} concentration of 4 mM, indicating that the peptide extremities are not deeply buried within the SDS micelle. Therefore, perpendicular orientations of the peptides with respect to the surface of SDS micelles can be dismissed. Antp and Hox peptides exhibit comparable behaviors regarding segment 45−49, which contains two aliphatic and two aromatic residues, with position 46 being occupied by a polar residue. Indeed, these residues show the weakest decays of $HN-H^\alpha$ cross-peaks compared to other

residues. The Eng peptide slightly differs from the former two peptides because, in addition to this segment, residues 51−55 also exhibit HN−H^{α} correlations at the largest Mn^{2+} concentration tested. The Kno peptide differs from the other three peptides because the less severely affected residues are basic residues localized in positions 54 and 55.

To get more quantitative information on the localization within the micelle, the enhancements of proton relaxation induced by the same range of Mn^{2+} concentrations were also analyzed on SDS and small organic molecules solubilized in SDS micelles. The transverse relaxation rate enhancements were measured by analyzing the line width at half-height $\Delta\nu_{1/2}$ of the proton resonances that are well-resolved in 1D spectra. The addition of Mn^{2+} causes a linear increase of the line width of SDS resonances, with protons closer to the sulfate headgroup being more broadened. The different sensitivities to the paramagnetic probe were evaluated by calculating the molar relaxivities S_P, defined as the slopes of plots of $\Delta\nu_{1/2}$ versus the Mn^{2+} concentration (*39*). The measured S_P parameters are 26.3, 13.1, and 3.7 Hz mM^{-1} for H1, H2, and H12 protons of SDS, respectively. The paramagnetic enhancements were also analyzed on sodium cinnamate ($C_6H_5-CH{=}CH-COO^-\ Na^+$) in a SDS micelle, which was selected for its amphipathic nature and its conformational rigidity. The S_P factors are 41 and 26 for the ethylenic protons in α and β positions, respectively, and 3.4, 1.2, and 1.3 for the aromatic protons in ortho, meta, and para positions, respectively. The relaxivities observed for cinnamate show that this molecule is embedded within SDS micelles, with the carboxylate group occupying a position close to the sulfate group of SDS in micelles. From the weaker paramagnetic enhancements observed for the aromatic protons of cinnamate, it can be deduced that the phenyl moiety is more deeply buried. Taking a SDS micelle radius of ∼22 Å and a long axis for cinnamate of ∼8 Å, the meta/para protons would be localized around 14−15 Å from the micelle mass center, corresponding approximately to the C3 and C4 methylene positions in the SDS molecule (assuming an all trans conformation). The paramagnetic enhancements were also analyzed on 2D TOCSY spectra. The SDS cross-peaks corresponding to H1/H2 and H2/H3 correlations disappear for Mn^{2+} concentrations of ∼0.5 and ∼1 mM, respectively. The correlations between H11 and H12 protons of SDS and between aromatic protons of cinnamate are still observed at 4 mM Mn^{2+}. These results indicate that the paramagnetic enhancements induced by Mn^{2+}, as monitored by TOCSY experiments, concern mainly protons exposed on the micelle surface or located inside but close to the surface, in a region occupied by C1 and C2 methylene groups of SDS. The measured relaxivities show that protons lying deeper in the micelle should be much less affected by the Mn^{2+} probe, in the concentration range used (0.5−4 mM).

Measurement of the Cellular Uptake of the Cell-Penetrating Peptides by MALDI−TOF MS. The amount of internalized cell-penetrating peptide can be measured by MALDI−TOF MS with a method recently developed in our group. The method gives directly the total amount of intact intracellular peptide and allows characterization of eventual CPP digests (*17*). The quantification of the internalized CPP by MALDI−TOF MS is achieved by using an internal standard with the same sequence and labeled with a stable isotope (deuterium). The CPPs are functionalized on their N terminus by a biotin and an isotope tag composed of four nondeuterated glycine residues for the internalized species (H-CPP) and four deuterated glycine residues for the standard (D-CPP) (Table 1). A known amount of standard is added at the end of the cell incubation with the H-CPP just prior to lysis. The biotinylated peptides are then easily recovered, concentrated, and desalted using streptavidin-coated magnetic beads to allow the analysis by MALDI−TOF MS. Because both H-CPP and D-CPP have the same sequence, they exhibit the same efficiency of desorption/ionization by MALDI−TOF MS and the relative intensity of their signals on the mass spectra corresponds to their relative proportion in the sample. The amount of intact internalized peptide is thus calculated from the area ratio of the H-CPP and D-CPP signals ($[M + H]^+$ ions).

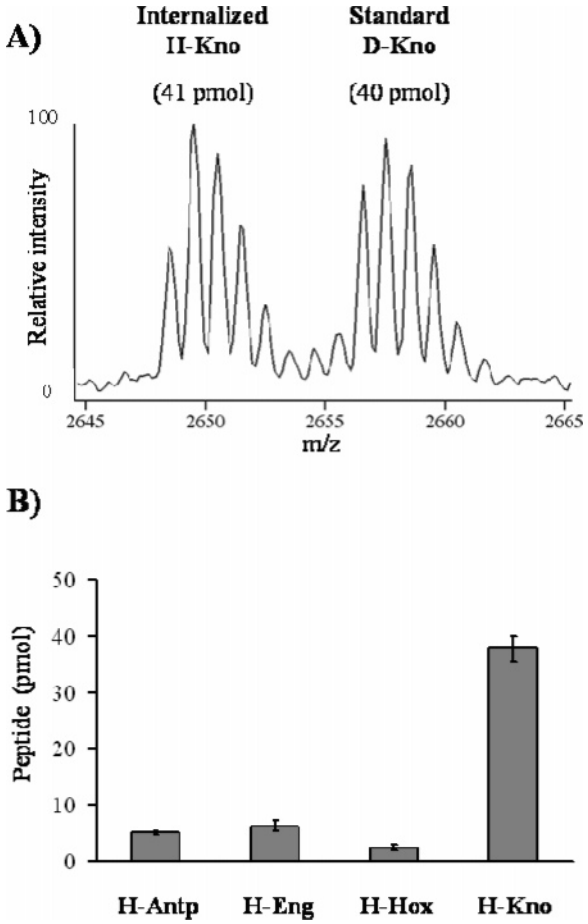

FIGURE 5: (A) MALDI−TOF mass spectrum obtained for H-Kno internalization. The spectrum shows the $[M + H]^+$ peaks of intact H-Kno and D-Kno. The total areas of the $[M + H]^+$ peaks including all isotopes were used for quantification. (B) Comparison of the amount of intact internalized CPP. Results correspond to the total amount of CPP internalized in 10^6 CHO cells. Each data is the average result of at least four independent experiments performed in duplicates ± SEM.

Using this method, we measured the amount of internalized peptide for the four different CPPs incubated with 10^6 CHO cells for 1.25 h at 37 °C at a concentration of 7.5 μM (Figure 5). H-Kno gave the highest intracellular peptide amount with 37.8 ± 2.3 pmol [mean value ± standard error of the mean (SEM), $n = 8$] in 10^6 cells. This corresponds to an estimated intracellular concentration of 25.2 ± 1.5 μM based on a volume per cell of 1.5 pL. H-Eng and H-Antp gave results close to each other, leading to intracellular concentrations

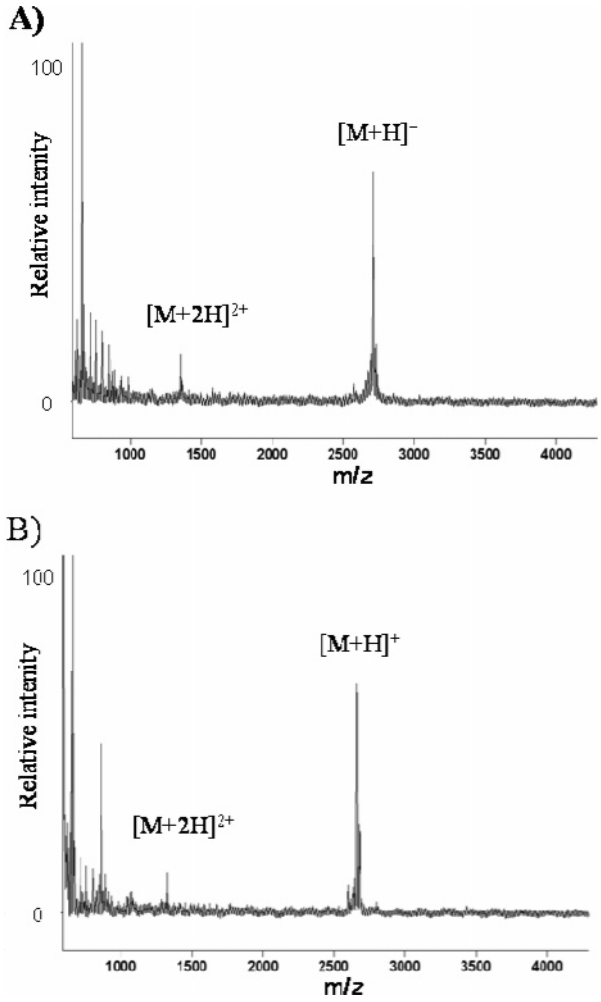

FIGURE 6: (A) MALDI−TOF mass spectrum of H-Antp incubated with CHO cells for 5 h. (B) MALDI−TOF mass spectrum of H-Kno incubated with CHO cells for 1.25 h. The $[M + H]^+$ and $[M + 2H]^{2+}$ peaks of intact H-CPP and D-CPP are observed. The peaks in the *m*/*z* range below 1000 correspond to the matrix and polymer covering the streptavidin-coated magnetic beads.

of 4.2 ± 0.7 μM (n = 8) and 3.4 ± 0.2 μM (n = 12), respectively. The lowest intracellular concentration was obtained for H-Hox corresponding to 1.7 ± 0.3 μM (n = 8). In all cases, the results were very reproducible. No peaks corresponding to an intracellular degradation were detected for H-Antp on the mass spectra. When the peptide was incubated with CHO cells for 5 h instead of 75 min, no degradation was observed either (Figure 6A) and the intracellular peptide concentration was not significantly changed. Similarly, H-Kno was not degraded after 75 min (Figure 6B). Two digests were observed in the mass spectra obtained for the cellular uptake of H-Hox and occasionally H-Eng. In both cases, the digests corresponded to the loss of the last or last three residues (on the peptide C terminus) and gave less intense signals than the intact peptide (see Figure S1 in the Supporting Information).

DISCUSSION

Positioning Models as Inferred by the Titration with the Mn^{2+} Probe. The localization of the four homeodomain-derived peptides in SDS micelles was investigated by using Mn^{2+} as a paramagnetic probe. Although this water-soluble probe is located outside the micelle, it is expected to accumulate near the anionic surface of the SDS micelle and to be uniformly distributed around the peptide/micelle complex. The increase of the Mn^{2+} concentration leads to the progressive broadening of resonances and disappearance of cross-peaks in 2D TOCSY spectra for protons located deeper in the micelle. The maximum Mn^{2+} concentration used corresponds to a ratio of 2 Mn^{2+} ions per SDS micelle. Under these conditions, paramagnetic enhancements measured on small organic molecules are weak for protons located about 8 Å from the surface. Interestingly, the molar relaxivity of the end-chain H12 proton of SDS is slightly higher than that observed for cinnamate aromatic protons. Although a much deeper position would be expected for an all trans alkyl chain, this result enlightens the dynamics of SDS chains within the micelle and shows that the distance of the closest approach to the paramagnetic cation can be much smaller. Indeed, the probability distribution of the terminal methyl group, calculated from a molecular dynamics simulation of the SDS micelle (*40*), is significant up to 5 Å from the micelle surface.

The paramagnetic effects induced by Mn^{2+} on peptide resonances were mainly analyzed on backbone HN−H^{α} cross-peaks in 2D TOCSY spectra because the side-chain dynamics will complicate the analysis of correlations involving side-chain protons. Furthermore, in the case of Lys and Arg side chains bearing a positive charge, putative electrostatic repulsion with Mn^{2+} might lead to a nonuniform distribution of Mn^{2+} around the peptide/SDS micelle complex and to weaker relaxation enhancements for protons in the vicinity of the cationic group. The observation of cross-peaks involving the H^{ϵ} protons of Lys residues at high Mn^{2+} concentrations (4 mM) suggests that this might be indeed the case. However, the increased distance between the backbone atoms and the side-chain charged group should limit the impact of Mn^{2+} electrostatic repulsion when analyzing backbone proton correlations. Indeed, the C-terminal regions of Antp and Hox peptides that are rich in cationic residues do not exhibit weak sensitivities for their backbone protons, indicating that putative repulsive effects should be negligible at the backbone level. Furthermore, the analysis of the paramagnetic relaxation enhancements for backbone protons of individual Arg and Lys residues in the four peptides shows large variations in sensitivities to the Mn^{2+} probe that are likely to reflect differences in accessibility.

The titration with Mn^{2+} showed that the four homeodomain-derived peptides exhibit different sensitivities to the paramagnetic probe, as evidenced by the decrease of 2D TOCSY cross-peak intensities. The N- and C-terminal residues of the four homeodomain-derived peptides are affected by the Mn^{2+} probe, indicating that the peptide extremities are located close to the surface. Therefore, the peptides do not adopt orientations perpendicular to the micelle surface. The different behaviors of the four peptides suggest variations in the depth of insertion in the micelle. The Mn^{2+} titrations carried on small molecules in the SDS micelle show that a region corresponding to the sulfate headgroup and the C1−C4 methylene groups of SDS is affected by the Mn^{2+} probe. The aromatic protons of cinnamate, whose position should be close to that of C3 and C4 methylene groups of SDS, are weakly affected by Mn^{2+} and show low relaxivities (S_P = 1−2 Hz mM^{-1}). Peptide

FIGURE 7: Schematic model of the position of Kno (left) and Eng (right) peptides with respect to SDS micelle. The inner and outer circles correspond to a radius of 16 and 22 Å, respectively.

backbone protons that give rise to correlations in the TOCSY spectra at 4 mM Mn^{2+} also show relaxivities of the same order. Nevertheless, a direct comparison of the relaxation enhancements cannot be drawn because of the differences of correlation times between small organic molecules and peptides. Larger relaxation enhancements will be expected for the peptide compared to the small molecule occupying a similar position in the micelle because of the differences in dynamics (*41*). Therefore, distances to the surface may be underestimated. A tentative model of the position of the most diverging Eng and Kno peptides is shown schematically in Figure 7 to illustrate the differences of accessibility to the probe. Although the immersion depth in the micelle may be underestimated, a deeper insertion in the hydrophobic interior of the micelle should be energetically unfavorable because the positively charged end groups of Arg and Lys side chains will tend to be solvated by the aqueous phase and interact with the anionic sulfate group of SDS.

Comparison of Positioning Models of Antp. Our positioning model of the Antp peptide in the SDS micelle, as inferred by Mn^{2+} titration data, differs markedly from the previously published model, in which Antp adopts a perpendicular orientation relative to the SDS micelle surface, with the C terminus located close to the center of the micelle (*35*). This previous model was based on the relaxation effects induced by the water-soluble Mn^{2+} ion as well as lipid-soluble doxyl-labeled stearic acids. The lower concentrations of Mn^{2+} used (0.3 equiv of Mn^{2+} ion per SDS micelle compared to 2 equiv in our study) did not allow the authors to detect the sensitivity of the C-terminal residues to the Mn^{2+} probe. It should be noted that the dynamics of lipid-soluble 5- and 12-doxyl-stearic acids makes the analysis of relaxation data gathered with these probes difficult. Indeed, it has been shown that 5- and 12-doxylstearic acids broaden all proton signals of SDS to some extent and can affect similar sets of resonances of peptides associated to a SDS micelle (*42*). This poor specificity can be ascribed to the high flexibility of these alkyl chains in the micelle interior. Furthermore, the possibility of specific interactions between the peptide and the doxyl group may also limit their applications for localizing peptides in micelles.

In contrast, our positioning model appears to be quite similar to the model of Antp in negatively charged bicelles obtained by Gräslund and co-workers (*37*), in which Antp is located parallel to the bicelle surface within the headgroup region. The helical secondary structure is also very similar in both environments. Therefore, although the SDS micelle is a very simplistic membrane-mimetic system, the micellar and bicellar environments yield similar results regarding the conformation and the position of the Antp peptide. A number of spectroscopic studies of Antp in various membrane environments have been reported and yield different results regarding Antp conformation and localization. Antp was found to interact mainly with the headgroup region of membrane bilayers in neutron reflectivity (*43*), plasmon-waveguide resonance (*44*) and polarized-light spectroscopy (*45*). However, at high peptide/lipid ratios and a high charge density, Antp was found to adopt mainly β structures (*46*, *47*) and causes membrane perturbation (*48*, *49*). A recent NMR study of Antp in membrane bicelles also revealed that the depth of peptide insertion and changes in anionic lipid orientation were concentration-dependent (*38*).

Interactions of the Four Homeodomain-Derived Peptides in the SDS Micellar Environment. NMR spectroscopy indicates that helical conformations of the peptides are induced in the presence of SDS micelles. The helical propensity of each peptide is correlated to the depth of insertion within the micelle. Indeed, Eng is the most buried peptide in the SDS micelle and also adopts the most stable helix as indicated by NMR parameters and structure calculations. Within each peptide, the central hydrophobic segment containing the two conserved Trp and Phe residues exhibits the highest helical propensity. The weaker helical propensity observed in the positively charged C-terminal part suggests that electrostatic interactions with the anionic headgroups of SDS are not sufficient to induce a stable helical secondary structure.

The analysis of Antp, Eng, and Hox positioning in SDS micelles indicates that the 45−49 segment is embedded in the micelle. This position is probably driven by interactions of hydrophobic Ile, Phe, and Trp side chains with lipid chains. The positively charged C-terminal residues are also inserted within the micelle but to a lesser extent. The comparison of relaxation effects induced by 4 mM Mn^{2+} on Trp side-chain protons of Antp shows that Trp56 is slightly more sensitive to the paramagnetic probe than Trp48 (data not shown). The increased exposure of Trp56 is in agreement with the differences in sensitivity observed at the backbone level between segment 45−49 and the C-terminal segment. A deeper insertion of Trp48 compared to Trp56 was also observed in negatively charged phospholipid vesicles, on the basis of intrinsic Trp fluorescence measurements on Antp and Antp analogues (*50*, *51*). In contrast to Antp, Eng, and Hox, the position of the Kno peptide is much closer to the surface, with the hydrophobic 48−50 segment not deeply inserted in the micelle. This result was unexpected, given the overall positive charge and the conservation of Trp48 and Phe49 residues.

Quantification of the CPP Internalization Efficiencies by MALDI−TOF MS. The CPP internalization efficiencies have been measured by MALDI−TOF MS employing a method that we have recently described. The method is based on the use of a standard with the same sequence as the CPP and labeled with a stable isotope (deuterium) to allow peptide quantification by MALDI−TOF MS. There are several problems associated with the measure of CPP cellular uptake that our experimental method has been designed to overcome to give reliable quantification (*17*). First, CPPs bind strongly to the cell surface and are not completely removed even by repeated washings. The methods to measure CPP internalization must distinguish between the external membrane-bound and the truly internalized peptide to avoid overestimation. In the methods presented in the literature, the external peptide is often submitted to enzymatic digestion (*52*, *53*). Alternatively, intracellular and membrane-associated CPP are dis-

tinguished by chemical modification of the external peptide (*54*) or by fluorescence quenching (*11*, *55*). Our protocol includes a step of trypsin digestion of the extracellular peptide. Digests are expected to have a reduced affinity for the cell membrane and to be removed by washing. However, if some of the peptide fragments retain affinity for the membrane and are not eliminated, they can be distinguished with this method from intracellular intact peptide and therefore do not interfere with quantification. This is an advantage over the CPP quantification methods based on the detection of a reporter group (fluorophore) and not on the direct detection of the peptide.

There are two other problems that have been addressed for the accuracy of the quantification. Because it is the amount of intact internalized peptide that is measured here using a standard, peptide degradation must be prevented during sample preparation. The heating step introduced in the protocol denatures proteases released during cell lysis. The standard, which is subjected to the entire process of cell lysis and peptide recovery, serves as a control of degradation. Results are only valid if no deuterated digests are detected on the mass spectra. In addition, discrimination between the internalized peptide and the standard must be prevented during peptide recovery by the streptavidin-coated beads. CPPs may bind to some of the components of the cell lysate, which may hamper their capture by the streptavidin-coated beads. The heating step allows both H-CPP and D-CPP, which have the same sequence, to be exposed to the same interacting species among lysate components. Both peptides are thus subsequently captured with the same efficiency and are found on the deposit analyzed by MALDI−TOF MS in the same proportions as in the lysate.

In addition to providing reliable uptake quantification, this method yields information about CPP degradation. In this study, fragments were only observed for Hox and occasionally for Eng but, in both cases, with a lower abundance compared to the intact peptide (Figure S1 in the Supporting Information). These fragments may have been produced inside cells. However, because only two digests are observed, resulting from the cleavage of the CPPs at the C terminus of basic residues, they more likely correspond to a membrane-bound peptide that has been degraded by trypsin but not completely eliminated by washing. For these CPPs, a small fraction of the peptide adsorbed on the cell surface may not be totally accessible to trypsin. We did not observe any intracellular degradation for Kno. Antp was not degraded either, even after 5 h of incubation with cells, and the intracellular concentration did not change significantly between 75 min and 5 h of incubation. The four peptides are not quickly degraded after internalization, showing that they are not directed to lysosomes within the incubation period. Several studies of the degradation inside cells of fluorophore-labeled penetratin by MALDI−TOF MS have been reported. Fischer et al. observed both intact and digested forms after 2 h of incubation with MC57 cells (*56*). Lindgren et al. also reported the rapid peptide degradation in Caco-2 cells, with some intact peptide still detectable after 4 h (*57*). The difference with our results may be explained by the use of different cell types or reporter groups (fluorophore versus biotin), which may lead to different degradation rates in the cells.

Comparison of Internalization Efficiencies and Interactions in Membrane Mimetic Systems. The four CPPs studied here gave significantly different results concerning the cellular uptake efficiency. The best result was obtained for Kno. Its intracellular concentration was 15 times higher than the concentration obtained for Hox. Moreover, Kno was the only peptide for which the concentration of intact peptide inside cells was greater than in the extracellular medium (∼3.5 times). Hox gave the lowest intracellular concentration, while Eng and Antp showed similar internalization efficiencies. Previous studies showed that the positive charges in the C-terminal domain of Antennapedia third helix are critical for internalization (*7*, *11*). In addition, the key role of Trp48 in the uptake of Antp has been established, whereas the role of Trp56 is more controversial (*7*, *11*−*13*). Noteworthy, Trp48 is conserved among all of the homeodomains but not Trp56. In comparison to Antp, Eng lacks the N-terminal basic residue and Trp56 is substituted by an Ile residue, but both peptides have a similar arrangement of hydrophilic and hydrophobic residues. The observation of similar uptake efficiencies for Antp and Eng suggests that Trp56 does not play a critical role in internalization as long as it is replaced by a hydrophobic residue. In contrast, the presence of an acidic residue in the C-terminal segment may be detrimental for cellular uptake, as evidenced by Hox translocation efficiency. Kno has the most divergent sequence. It contains two Trp residues such as Antp but a smaller number of basic residues (i.e., five Arg or Lys plus a His that is potentially protonated in acidic compartments such as endosomes, compared to seven Arg or Lys for Antp). However, in the case of Kno, the basic residues of the C-terminal segment are more clustered and are adjacent to a long N-terminal segment devoid of charged residues, compared to Antp and Eng. When these results are taken together, they suggest that it is the clustering of the basic residues in the C-terminal part that is more important for the uptake efficiency than the total number of positive charges.

It has been established that Arg residues play an important role in cellular uptake because Antp analogues in which all basic residues are either Arg or Lys residues have markedly different cell-binding and uptake properties (*58*). The examination of the four CPP sequences suggests that the differences in uptake efficiencies cannot be accounted for by variation in the number or the distribution of Arg residues. On the basis of molecular dynamics simulations of Antp in lipid bilayers (*59*), cation−π interactions between Arg and aromatic residues have been proposed to contribute to the insertion of the peptide into the lipid bilayer. Such interactions were indeed observed in our study between Trp48 and Arg52 and between Phe49 and Arg53 for the Antp peptide in SDS micelles. Similarly, the Phe49−Arg53 interaction is conserved in Eng, Hox, and Kno peptides. The side-chain interaction between Trp48 and the residue in position 52 also exists, but the Arg residue is replaced by Lys or Gln in the case of Eng and Kno peptides. Therefore, a cation−π interaction between residues 48 and 52 does not seem to be critical for homeodomain-derived peptide translocation because it is absent in Kno.

Surface Interactions. Our NMR results show that the four homeodomain-derived peptides adopt roughly parallel orientations relative to the SDS micelle surface. In particular, the orientation of Antp in the SDS micelle is quite similar

to that observed in negatively charged bicelles by NMR spectroscopy (*37*). Parallel orientations of Antp to the bilayer surface were also established by oriented circular dichroism (*49*) and linear dichroism (*45*). A large number of biophysical techniques indicated that Antp remains close to the water−lipid interface, including neutron reflectivity (*43*), Trp fluorescence (*49*, *51*), plasmon-waveguide resonance, and impedance spectroscopy (*44*).

Interestingly, the Kno peptide, which has the highest uptake efficiency, was found to be the closest to the surface in the micellar membrane-mimicking system. It also exhibits a weaker helical propensity, which is probably related to the more superficial insertion within the micelle. Noteworthy, the helical secondary structure is a consequence of the interaction with the membrane environment and does not seem to be required for membrane translocation, as shown by the use of nonhelical penetratin analogues (*9*).

The results obtained with this series of homeodomain-derived peptides converge with a previous NMR study of Antp and the nontranslocating [W48F, W56F]Antp analogue in a bicellar system (*37*). Indeed, the two peptides were found to adopt slightly different positions in the bilayer, with the translocating peptide lying closer to the surface. Therefore, a strong interaction with a membrane system does not seem to be required and might even be detrimental for efficient translocation. Electrostatic interactions near the membrane surface may be the major determinant in the binding and translocation processes (*59*, *60*).

The internalization mechanism of Antp is still controversial and may not even be unique. Because all of the peptides studied herein are derived from homeodomains, they are likely to share the same mechanism of cellular uptake. The different models proposed for Antp and other cationic CPPs fall into two categories: (i) direct cell-membrane translocation through transient formation of inverted micelles (*9*, *10*), a mechanism involving ion-pair complexes partitioning in the case of guanidinium-rich peptides (*61*) or an "electroporation-like mechanism" (*60*), and (ii) vesicle formation either by endocytosis (*56*, *62*, *63*) or macropinocytosis (*64*). Numerous studies have shown that cargoes delivered by cationic CPPs can reach their nuclear or cytosolic targets (*8*). Therefore, even in the case of vesicular uptake, a biological membrane has to be crossed. Whatever the mechanism of uptake, a peripheral surface positioning of cationic CPPs, as observed for Knotted, may trigger a transient destabilization of the bilayer to allow peptide translocation.

CONCLUDING REMARKS

Despite strong sequence conservation of homeodomains, the four selected homeodomain-derived peptides show subtle differences in the interaction with membrane mimetic systems and surprisingly strong variations in translocating efficiencies. This study yielded to the discovery of a new CPP, corresponding to the third helix of Knotted-1. This CPP has an improved efficiency in cellular uptake compared to penetratin and two homeodomain-derived peptides, as well as other cationic peptides including $(Arg)_9$ and Tat_{48-59} previously examined with the same mass spectrometry-based method (*17*). Work is in progress to study the efficiency of Knotted-1 third helix to deliver specific cargoes to relevant biological targets.

ACKNOWLEDGMENT

We thank Alain Joliot and Alain Prochiantz for fruitful discussions.

SUPPORTING INFORMATION AVAILABLE

Table S1, proton assignment of Antp peptide; Table S2, proton assignment of Eng peptide; Table S3, proton assignment of Hox peptide; Table S4, proton assignment of Kno peptide; Table S5, statistics of NMR structure families; Figure S1, digests observed in the cellular uptake experiments of H-Hox and H-Eng. This material is available free of charge via the Internet at http://pubs.acs.org.

REFERENCES

1. Gehring, W. J., Affolter, M., and Bürglin, T. (1994) Homeodomain proteins, *Annu. Rev. Biochem. 63*, 487−526.
2. Joliot, A., Pernelle, C., Deagostini-Bazin, H., and Prochiantz, A. (1991) Antennapedia homeobox peptide regulates neural morphogenesis, *Proc. Natl. Acad. Sci. U.S.A. 88*, 1864−1868.
3. Joliot, A., Maizel, A., Rosenberg, D., Trembleau, A., Dupas, S., Volovitch, M., and Prochiantz, A. (1998) Identification of a signal sequence necessary for the unconventional secretion of Engrailed homeoprotein, *Curr. Biol. 8*, 856−863.
4. Chatelin, L., Volovitch, M., Joliot, A. H., Perez, F., and Prochiantz, A. (1996) Transcription factor hoxa-5 is taken up by cells in culture and conveyed to their nuclei, *Mech. Dev. 55*, 111−117.
5. Prochiantz, A. (2000) Messenger proteins: Homeoproteins, TAT and others, *Curr. Opin. Cell. Biol. 12*, 400−406.
6. Noguchi, H., Kaneto, H., Weir, G. C., and Bonner-Weir, S. (2003) PDX-1 protein containing its own antennapedia-like protein transduction domain can transduce pancreatic duct and islet cells, *Diabetes 52*, 1732−1737.
7. Derossi, D., Joliot, A. H., Chassaing, G., and Prochiantz, A. (1994) The third helix of the Antennapedia homeodomain translocates through biological membranes, *J. Biol. Chem. 269*, 10444−10450.
8. Dietz, G. P., and Bahr, M. (2004) Delivery of bioactive molecules into the cell: The Trojan horse approach, *Mol. Cell Neurosci. 27*, 85−131.
9. Derossi, D., Calvet, S., Trembleau, A., Brunissen, A., Chassaing, G., and Prochiantz, A. (1996) Cell internalization of the third helix of the Antennapedia homeodomain is receptor-independent, *J. Biol. Chem. 271*, 18188−18193.
10. Berlose, J. P., Convert, O., Derossi, D., Brunissen, A., and Chassaing, G. (1996) Conformational and associative behaviours of the third helix of Antennapedia homeodomain in membrane-mimetic environments, *Eur. J. Biochem. 242*, 372−386.
11. Drin, G., Mazel, M., Clair, P., Mathieu, D., Kaczorek, M., and Temsamani, J. (2001) Physico-chemical requirements for cellular uptake of pAntp peptide. Role of lipid-binding affinity, *Eur. J. Biochem. 268*, 1304−1314.
12. Fischer, P. M., Zhelev, N. Z., Wang, S., Melville, J. E., Fahraeus, R., and Lane, D. P. (2000) Structure−activity relationship of truncated and substituted analogues of the intracellular delivery vector penetratin, *J. Pept. Res. 55*, 163−172.
13. Le Roux, I., Joliot, A. H., Bloch-Gallego, E., Prochiantz, A., and Volovitch, M. (1993) Neurotrophic activity of the Antennapedia homeodomain depends on its specific DNA-binding properties, *Proc. Natl. Acad. Sci. U.S.A. 90*, 9120−9124.
14. Kilk, K., Magzoub, M., Pooga, M., Eriksson, L. E., Langel, U., and Gräslund, A. (2001) Cellular internalization of a cargo complex with a novel peptide derived from the third helix of the islet-1 homeodomain. Comparison with the penetratin peptide, *Bioconjugate Chem. 12*, 911−916.
15. Noguchi, H., Matsushita, M., Matsumoto, S., Lu, Y. F., Matsui, H., and Bonner-Weir, S. (2005) Mechanism of PDX-1 protein transduction, *Biochem. Biophys. Res. Commun. 332*, 68−74.
16. Tassetto, M., Maizel, A., Osorio, J., and Joliot, A. (2005) Plant and animal homeodomains use convergent mechanisms for intercellular transfer, *EMBO Rep. 6*, 885−890.
17. Burlina, F., Sagan, S., Bolbach, G., and Chassaing, G. (2005) Quantification of the cellular uptake of cell-penetrating peptides by MALDI−TOF mass spectrometry, *Angew. Chem. Int. Ed. 44*, 4244−4247.

18. Bartels, C., Xia, T.-H., Billeter, M., Güntert, P., and Wüthrich, K. (1995) The program XEASY for computer-supported NMR spectral analysis of biological macromolecules, *J. Biomol. NMR 6*, 1−10.
19. Davis, D. G., and Bax, A. (1985) Assignment of complex proton NMR spectra via two-dimensional homonuclear Hartmann−Hahn spectroscopy, *J. Am. Chem. Soc. 107*, 2820−2821.
20. Griesinger, C., Otting, G., Wüthrich, K., and Ernst, R. R. (1988) Clean TOCSY for proton spin system identification in macromolecules, *J. Am. Chem. Soc. 110*, 7870−7872.
21. Kumar, A., Ernst, R. R., and Wüthrich, K. (1980) A two-dimensional nuclear Overhauser enhancement (2D NOE) experiment for the elucidation of complete proton−proton cross-relaxation networks in biological macromolecules, *Biochem. Biophys. Res. Commun. 95*, 1−6.
22. Lippens, G., Dhalluin, C., and Wieruszeski, J. M. (1995) Use of a water flip-back pulse in the homonuclear NOESY experiment, *J. Biomol. NMR 5*, 327−331.
23. Sklenar, V., Piotto, M., Leppik, R., and Saudek, V. (1993) Gradient-tailored water suppression for proton-nitrogen-15 HSQC experiments optimized to retain full sensitivity, *J. Magn. Reson. A 102*, 241−245.
24. Rance, M., Sørensen, O. W., Bodenhausen, G., Wagner, G., Ernst, R. R., and Wüthrich, K. (1983) Improved spectral resolution in COSY proton NMR spectra of proteins via double quantum filtering, *Biochem. Biophys. Res. Commun. 117*, 479−485.
25. Szyperski, T., Güntert, P., Otting, G., and Wüthrich, K. (1992) Determination of scalar coupling constants by inverse Fourier transformation of in-phase multiplets, *J. Magn. Reson. 99*, 552−560.
26. Wishart, D. S., Bigam, C. G., Holm, A., Hodges, R. S., and Sykes, B. D. (1995) ^{1}H, ^{13}C and ^{15}N random coil NMR chemical shifts of the common amino acids. I. Investigations of nearest-neighbor effects, *J. Biomol. NMR 5*, 67−81.
27. Wüthrich, K., Billeter, M., and Braun, W. (1983) Pseudo-structures for the 20 common amino acids for use in studies of protein conformations by measurements of intramolecular proton−proton distance constraints with nuclear magnetic resonance, *J. Mol. Biol. 169*, 949−961.
28. Ludvigsen, S., and Poulsen, F. M. (1992) Positive φ-angles in proteins by nuclear magnetic resonance spectroscopy, *J. Biomol. NMR 2*, 227−233.
29. Güntert, P., Mumenthaler, C., and Wüthrich, K. (1997) Torsion angle dynamics for NMR structure calculation with the new program DYANA, *J. Mol. Biol. 273*, 283−298.
30. Schwieters, C. D., Kuszewski, J. J., Tjandra, N., and Clore, M. G. (2003) The Xplor-NIH NMR molecular structure determination package, *J. Magn. Reson. 160*, 65−73.
31. Laskowski, R. A., Rullmannn, J. A., MacArthur, M. W., Kaptein, R., and Thornton, J. M. (1996) AQUA and PROCHECK-NMR: Programs for checking the quality of protein structures solved by NMR, *J. Biomol. NMR 8*, 477−486.
32. Damberg, P., Jarvet, J., and Gräslund, A. (2001) Micellar systems as solvents in peptide and protein structure determination, *Methods Enzymol. 339*, 271−285.
33. Wüthrich, K. (1986) *NMR of Proteins and Nucleic Acids*, Wiley, New York.
34. Czajlik, A., Mesko, E., Penke, B., and Perczel, A. (2002) Investigation of penetratin peptides. Part 1. The environment dependent conformational properties of penetratin and two of its derivatives, *J. Pept. Sci. 8*, 151−171.
35. Lindberg, M., and Gräslund, A. (2001) The position of the cell penetrating peptide penetratin in SDS micelles determined by NMR, *FEBS Lett. 497*, 39−44.
36. Andersson, A., Almqvist, J., Hagn, F., and Mäler, L. (2004) Diffusion and dynamics of penetratin in different membrane mimicking media, *Biochim. Biophys. Acta 1661*, 18−25.
37. Lindberg, M., Biverstahl, H., Gräslund, A., and Mäler, L. (2003) Structure and positioning comparison of two variants of penetratin in two different membrane mimicking systems by NMR, *Eur. J. Biochem. 270*, 3055−3063.
38. Zhang, W., and Smith, S. O. (2005) Mechanism of penetration of antp(43−58) into membrane bilayers, *Biochemistry 44*, 10110−10118.
39. Niccolai, N., Bonci, A., Rustici, M., Scarselli, M., Neri, P., Esposito, G., Mascagni, P., Motta, A., and Molinari, H. (1991) NMR delineation of inner and outer protons from paramagnetic relaxation perturbations in 1D and 2D spectra of peptides, *J. Chem. Soc., Perkin Trans. 2*, 1453−1457.
40. MacKerell, A. D., Jr. (1995) Molecular dynamics simulation analysis of a sodium dodecyl sulfate micelle in aqueous solution: Decreased fluidity of the micelle hydrocarbon interior, *J. Phys. Chem. 99*, 1846−1855.
41. Buffy, J. J., Hong, T., Yamaguchi, S., Waring, A. J., Lehrer, R. I., and Hong, M. (2003) Solid-state NMR investigation of the depth of insertion of protegrin-1 in lipid bilayers using paramagnetic Mn^{2+}, *Biophys. J. 85*, 2363−2373.
42. Jarvet, J., Zdunek, J., Damberg, P., and Gräslund, A. (1997) Three-dimensional structure and position of porcine motilin in sodium dodecyl sulfate micelles determined by ^{1}H NMR, *Biochemistry 36*, 8153−8163.
43. Fragneto, G., Graner, F., Charitat, T., Dubos, P., and Bellet-Amalric, E. (2000) Interaction of the third helix of Antennapedia homeodomain with a deposited phospholipid bilayer: A neutron reflectivity structural study, *Langmuir 16*, 4581−4588.
44. Salamon, Z., Lindblom, G., and Tollin, G. (2003) Plasmon-waveguide resonance and impedance spectroscopy studies of the interaction between penetratin and supported lipid bilayer membranes, *Biophys. J. 84*, 1796−1807.
45. Brattwall, C. E. B., Lincoln, P., and Norden, B. (2003) Orientation and conformation of cell-penetrating peptide penetratin in phospholipid vesicle membranes determined by polarized-light spectroscopy, *J. Am. Chem. Soc. 125*, 14214−14215.
46. Magzoub, M., Kilk, K., Eriksson, L. E. G., Langel, U., and Gräslund, A. (2001) Interaction and structure induction of cell-penetrating peptides in the presence of phospholipid vesicles, *Biochim. Biophys. Acta 1512*, 77−89.
47. Magzoub, M., Eriksson, L. E. G., and Gräslund, A. (2002) Conformational states of the cell-penetrating peptide penetratin when interacting with phospholipid vesicles: Effects of surface charge and peptide concentration, *Biochim. Biophys. Acta 1563*, 53−63.
48. Persson, D., Thoren, P. E., and Norden, B. (2001) Penetratin-induced aggregation and subsequent dissociation of negatively charged phospholipid vesicles, *FEBS Lett. 505*, 307−312.
49. Magzoub, M., Eriksson, L. E. G., and Gräslund, A. (2003) Comparison of the interaction, positioning, structure induction and membrane perturbation of cell-penetrating peptides and non-translocating variants with phospholipid vesicles, *Biophys. Chem. 103*, 271−288.
50. Christiaens, B., Symoens, S., Vanderheyden, S., Engelborghs, Y., Joliot, A., Prochiantz, A., Vandekerckhove, J., Rosseneu, M., and Vanloo, B. (2002) Tryptophan fluorescence study of the interaction of penetratin peptides with model membranes, *Eur. J. Biochem. 269*, 2918−2926.
51. Christiaens, B., Grooten, J., Reusens, M., Joliot, A., Goethals, M., Vandekerckhove, J., Prochiantz, A., and Rosseneu, M. (2004) Membrane interaction and cellular internalization of penetratin peptides, *Eur. J. Biochem. 271*, 1187−1197.
52. Lindgren, M., Gallet, X., Soomets, U., Hällbrink, M., Brakenhielm, E., Pooga, M., Brasseur, R., and Langel, U. (2000) Translocation properties of novel cell penetrating transportan and penetratin analogues, *Bioconjugate Chem. 11*, 619−626.
53. Richard, J. P., Melikov, K., Vives, E., Ramos, C., Verbeure, B., Gait, M. J., Chernomordik, L. V., and Lebleu, B. (2003) Cell-penetrating peptides. A reevaluation of the mechanism of cellular uptake, *J. Biol. Chem. 278*, 585−590.
54. Oehlke, J., Scheller, A., Wiesner, B., Krause, E., Beyermann, M., Klauschenz, E., Melzig, M., and Bienert, M. (1998) Cellular uptake of an α-helical amphipathic model peptide with the potential to deliver polar compounds into the cell interior non-endocytically, *Biochim. Biophys. Acta 1414*, 127−139.
55. Hällbrink, M., Floren, A., Elmquist, A., Pooga, M., Bartfai, T., and Langel, U. (2001) Cargo delivery kinetics of cell-penetrating peptides, *Biochim. Biophys. Acta 1515*, 101−109.
56. Fischer, R., Köhler, K., Fotin-Mleczek, M., and Brock, R. (2004) A stepwise dissection of the intracellular fate of cationic cell-penetrating peptides, *J. Biol. Chem. 279*, 12625−12635.
57. Lindgren, M. E., Hällbrink, M. M., Elmquist, A. M., and Langel, U. (2004) Passage of cell-penetrating peptides across a human epithelial cell layer *in vitro*, *Biochem. J. 377*, 69−76.
58. Thoren, P. E., Persson, D., Isakson, P., Goksor, M., Onfelt, A., and Norden, B. (2003) Uptake of analogs of penetratin, Tat(48−60) and oligoarginine in live cells, *Biochem. Biophys. Res. Commun. 307*, 100−107.
59. Lensink, M. F., Christiaens, B., Vandekerckhove, J., Prochiantz, A., and Rosseneu, M. (2005) Penetratin-membrane association:

W48/R52/W56 shield the peptide from the aqueous phase, *Biophys. J. 88*, 939−952.

60. Binder, H., and Lindblom, G. (2003) Charge-dependent translocation of the Trojan peptide penetratin across lipid membranes, *Biophys. J. 85*, 982−995.
61. Rothbard, J. B., Jessop, T. C., Lewis, R. S., Murray, B. A., and Wender, P. A. (2004) Role of membrane potential and hydrogen bonding in the mechanism of translocation of guanidinium-rich peptides into cells, *J. Am. Chem. Soc. 126*, 9506−9507.
62. Drin, G., Cottin, S., Blanc, E., Rees, A. R., and Temsamani, J. (2003) Studies on the internalization mechanism of cationic cell-penetrating peptides, *J. Biol. Chem. 278*, 31192−31201.
63. Richard, J. P., Melikov, K., Brooks, H., Prevot, P., Lebleu, B., and Chernomordik, L. V. (2005) Cellular uptake of unconjugated TAT peptide involves clathrin-dependent endocytosis and heparan sulfate receptors, *J. Biol. Chem. 280*, 15300−15306.
64. Wadia, J. S., Stan, R. V., and Dowdy, S. F. (2004) Transducible TAT-HA fusogenic peptide enhances escape of TAT-fusion proteins after lipid raft macropinocytosis, *Nat. Med. 10*, 310−315.

BI0518390